**REVIEW**

Check for updates

# Immobilization of metals on carbon nanotubes through non-covalent approaches – focus on the use of polymerized lipidic interfaces to prepare catalytic hybrids

Edmond Gravel, [ID] *[a] Mateus P. Nunes, [ID] [a,b] Snehal Pednekar, [ID] [a,c] Céline Demeese,[a] Guilherme A. M. Jardim, [ID] [b] Eufrânio N. da Silva Júnior, [ID] *[b] Irishi N. N. Namboothiri [ID] *[c] and Eric Doris [ID] *[a]

This review highlights advanced strategies for the immobilization of metal catalysts on carbon nanotubes, emphasizing non-covalent approaches and, in particular, polymerized lipidic coatings developed by our group. Such coatings provide a robust and modular interface for immobilizing catalytically active metal species, without compromising the structural and electronic integrity of the carbonaceous scaffold. Diacetylene-based amphiphiles self-assemble into hemi-micellar rings around nanotubes *via* hydrophobic effects and can be photopolymerized into stable structures that resist solvents, heat, and recycling. In this review, we describe how these polymerized lipid coatings serve as primary organic layers to enable dense and robust loading of catalytic metal species. The resulting nanohybrids deliver state-of-the-art catalytic metrics under exceptionally mild and sustainable conditions; for example, gold-nanotube hybrids catalyze silane oxidations at room temperature, in air, at metal loadings as low as 0.001 mol%, reaching turnover numbers up to 72 000 and turnover frequencies of 12 000 h$^{-1}$, while remaining readily recyclable. By integrating nano-confined reaction environments, non-destructive carbon nanotube functionalization and layer-by-layer interfacial design, polymerized lipid nanorings emerge as a versatile platform to bridge the gap between homogeneous and heterogeneous catalysis and engineer recyclable nanotube-based catalysts for organic synthesis and energy-related applications.

## Introduction

### Structure of carbon nanotubes

The discovery of carbon nanotubes (CNTs) is commonly attributed to Iijima of NEC corporation in the 1990s.[1] However, hints of their existence were already present in earlier studies such as the discovery of hollow graphitic carbon fibers by Radushkevich and Lukyanovich in 1952[2] and the work of Endo in 1976.[3] Since then, CNTs have attracted considerable interest in the field of nanotechnologies due to their unique properties. Carbon nanotubes were described for the first time at the atomic level in 1991 and their structure is now well established. The formation of a CNT can be seen as the result of a sheet of graphene rolling up on itself, creating a hollow cylinder, ideally made of only sp$^2$-hybridized carbon atoms (Fig. 1). Depending on the number of sheets rolled in successive layers, a distinction is made between single-layer nanotubes (single-walled carbon nanotubes – SWCNTs) and multilayer nanotubes (multi-walled carbon nanotubes – MWCNTs). While the former family is represented by a range of similar structures that mostly differ in their chirality (vector around which the graphene sheet is rolled up), the latter includes
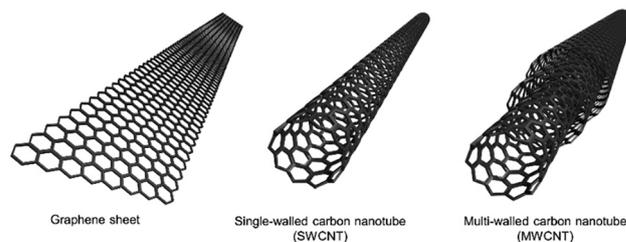


**Fig. 1** Structure of a graphic sheet and of different types of carbon nanotubes.

*[a]Université Paris-Saclay, CEA, INRAE, Département Médicaments et Technologies, pour la Santé (DMTS), SCBM, 91191 Gif-sur-Yvette, France. E-mail: edmond.gravel@cea.fr, eric.doris@cea.fr*
*[b]Departamento de Química, UFMG, Belo Horizonte, MG 31270-901, Brazil. E-mail: eufranio@ufmg.br*
*[c]Department of Chemistry, Indian Institute of Technology Bombay, Mumbai 400 076, India. E-mail: irishi@iitb.ac.in*

3220 | *Inorg. Chem. Front.*, 2026, **13**, 3220–3236

This journal is © the Partner Organisations 2026

diverse morphologies such as double-walled carbon nanotubes or herringbone carbon nanotubes (*i.e.* nanofibers), for instance. Nanotubes can be several micrometers long, with diameters typically ranging from 1 to 5 nanometers for SWCNTs, and several tens of nanometers for MWCNTs. The main techniques used to synthesize carbon nanotubes involve either high temperature processes such as sublimation of graphite under an inert atmosphere (arc discharge process) or laser ablation of a metal-doped graphite target; or medium-temperature processes such as the decomposition of a carbon-containing gas by metal catalysts (chemical vapor deposition).

## Properties

Thanks to their quasi-one-dimensional structure, CNTs exhibit a set of unique properties. Mechanically, their tensile strength and high Young's modulus make them strong and stiff while remaining lightweight and flexible. In terms of electronic behavior, chirality and diameter play an essential role in SWCNTs' properties, leading to either metallic nanotubes with very low resistivity and high current-carrying capacity or semiconducting ones with well-defined bandgaps (Fig. 2). On the other hand, MWCNTs mostly behave as metallic species.

SWCNTs also exhibit intrinsic optical properties, which depend on their chirality, leading to sharp absorption and photoluminescence features, including those in the near-infrared region. From a chemical perspective, even though the graphitic sidewalls of CNTs are relatively inert, they can be functionalized either covalently or non-covalently to improve solubility, compatibility with matrices, or enable attachment of molecules for composite, catalysis, or biomedical applications (Fig. 3).

## Applications

**Electronics.** At low temperatures, CNTs behave as superconductors[4] and incorporation into superconducting materials significantly influences CNTs' properties, mainly in terms of flux densities and pinning mechanisms.[5] Nanotubes have also been integrated into electronic circuits to produce diodes and transistors,[6] and used as a source of electrons[7] for the production of flat-panel displays.[8,9]

**Materials.** With a longitudinal elastic modulus of around 1 TPa, CNTs exhibit great mechanical strength that has been exploited for the assembly of composite materials reinforced with carbon nanotubes, valuable in various fields, such as sports equipment,[10] aeronautics and construction.[11,12]

**Medicine.** The electrical conductivity of SWCNTs is highly sensitive to the environment in which they are immersed and
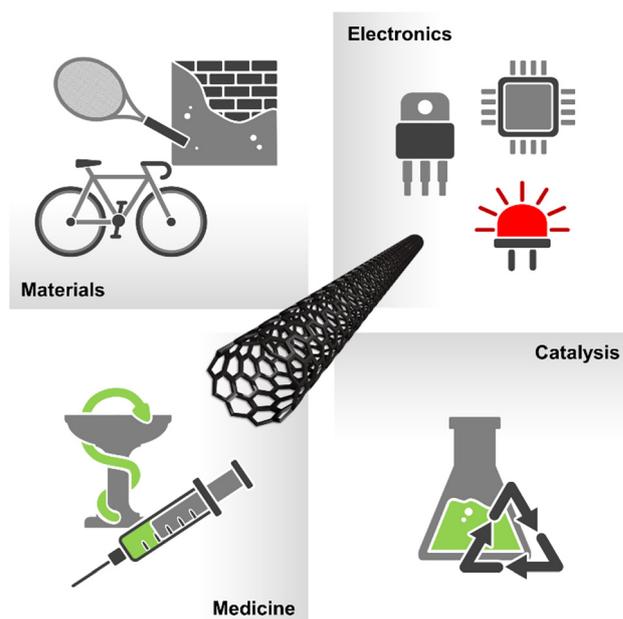


**Fig. 3** Fields of application of carbon nanotubes.

to the presence of species adsorbed on their surface. Nanotubes can thus convert local disturbances into detectable signals, enabling the design of CNT-based chemical[13] or biological[14] sensors. Another potential field of application for nanotubes is nanomedicine,[15,16] where they are used as platforms for loading and transport of active molecules within the body in preclinical studies.[17] Yet, the potential toxicity of CNTs is currently hindering specific developments in nanomedicine.

**Catalysis.** Carbon nanotubes have also recently emerged as a promising alternative to conventional catalyst supports as they provide some unique advantages such as low cost, chemical/thermal/mechanical stability, inertness, high specific surface area, chemically tunable topography, and facile reclaim.

The use of carbon nanotubes as a support of metals in heterogeneous catalysis has garnered much attention as they are consistent materials, which show catalytic properties superior to those of catalysts supported on other forms of materials. CNTs could also enhance the electron transfer rate of redox reactions and stabilize transient higher oxidation states of the supported metals.[18,19] These intrinsic properties make CNTs attractive platforms for the deposition of catalytic species with excellent dispersion and high surface area. Numerous examples of metal nanoparticles on CNTs have been described in the literature for heterogeneous catalytic applications.[20]

## Functionalization

All the applications mentioned above require the ability to manipulate carbon nanotubes, which are highly insoluble in most liquid media (organic or aqueous). This problem can be circumvented by chemically functionalizing CNTs,[21] to facilitate their dispersion, purification and characterization.
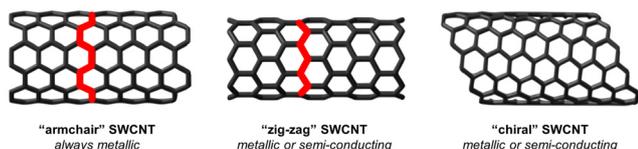


**Fig. 2** Effect of chirality on the electronic properties of SWCNTs.

"armchair" SWCNT
*always metallic*

"zig-zag" SWCNT
*metallic or semi-conducting*

"chiral" SWCNT
*metallic or semi-conducting*

This journal is © the Partner Organisations 2026

*Inorg. Chem. Front.*, 2026, **13**, 3220–3236 | **3221**

Functionalization provides anchoring points for the grafting of molecules of interest and can impart new properties to the nanotubes.

There are two main strategies for functionalizing the surface of CNTs, covalent and non-covalent. For example, covalent functionalization[22] can be achieved through the carboxylic acid groups generated on the surface of CNTs following oxidative treatment of the nanotubes. These carboxyl groups serve as attachment points for molecules of interest *via* coupling reactions (Fig. 4a). Covalent functionalization can also be achieved by generating highly reactive species in the medium (radicals,[23,24] carbenes,[25] nitrenes,[26] ylides,[27] or strong nucleophiles) which covalently react with the surface of the nanotubes and introduce functional sites (Fig. 4b [28] and Fig. 4c).[29]

The primary advantage of covalent functionalization is the strong attachment of functional groups at the surface of CNTs. However, this approach disrupts the sp$^2$-hybridized π-extended network of CNTs, leading to defects in the nanotube structure. As a result, intrinsic properties such as electrical conductivity, mechanical strength, and optical performance are often significantly degraded, limiting the suitability of covalently functionalized CNTs for applications that rely on pristine characteristics.

Non-covalent approaches, on the other hand, result from surface adsorption of polymers, lipids or polyaromatic compounds *via* van der Waals, electrostatic, π–π or hydrophobic effect-driven interactions, without altering the underlying carbon lattice (Fig. 4d–f). Non-covalent methods preserve intact the native surface of nanotubes as the sp$^2$ carbon framework is not affected by chemical transformations. These methods thus avoid the creation of defect sites that can act as recombination centers, and maintain high electrical conductivity, mechanical integrity and high specific surface area. Although the interactions involved in non-covalent supramolecular approaches are relatively weak and reversible, they provide dense decoration that can help improve dispersibility and accessibility of active sites in liquid media, and enable modulation of the local microenvironment (polarity, charge, and hydrophobicity). Non-covalent approaches thus allow the preservation of all key features of the carbonaceous nanomaterial that may be valuable in a catalytic context.

With this feature in mind, and as part of our longstanding interest in heterogeneous catalytic systems based on carbon nanotube platforms, we survey in this paper the various non-covalent approaches that were developed in the literature for the immobilization of metals endowed with catalytic properties on CNTs. A key focus is on polymerized lipidic interfaces developed by our group to link the active catalytic metal to CNTs, as this approach combines the best of both covalent and non-covalent worlds.

# Non-covalent functionalization of CNTs for metal immobilization

## π–π interactions

Among the different strategies for non-covalent immobilization of metal species on CNTs, π–π interactions are the most common. This approach takes advantage of the extended π-conjugated network at the surface of CNTs to anchor (poly) aromatic ligands or metal complexes. Different π-systems can be used to favor the interactions with the graphene-type surface of CNTs. For instance, López-Garzón *et al.* have developed azamacrocyclic metal ligands linked to a pyrimidine-based region that binds to the CNT through π–π interactions (Fig. 5a).[30] The authors showed that such ligands could be used for the immobilization of Pd on different carbonaceous supports, including CNTs, and the obtained hybrids were used as catalysts in the copper-free Sonogashira cross-coupling reaction.[31,32]

To promote stronger π–π interactions with the tube's surface, pyrene-derived moieties can be introduced and con-
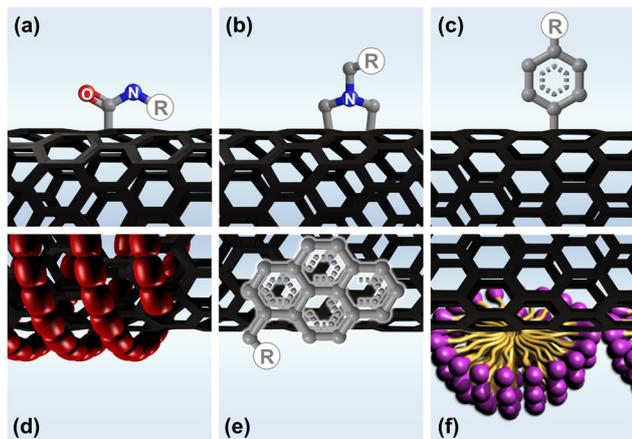


Fig. 4 Main routes for the functionalization of CNTs. Covalent approaches: (a) amide formation after surface oxidation; (b) 1,3-dipolar cycloaddition; and (c) radical addition. Non-covalent approaches: (d) polymer wrapping; (e) π-stacking; and (f) lipid assembly through a hydrophobic effect.
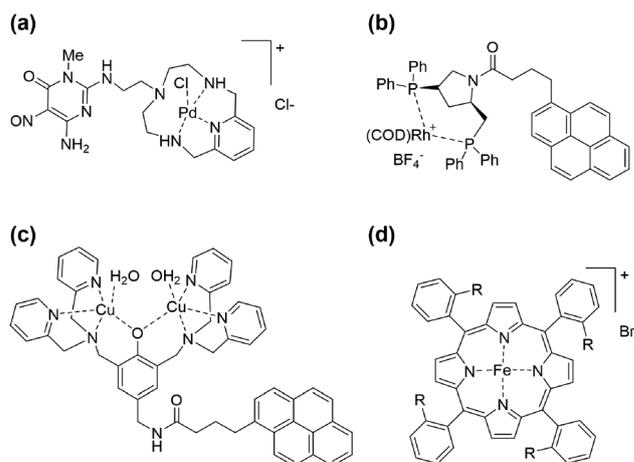


Fig. 5 Examples of (a) palladium; (b) rhodium; (c) copper; and (d) iron complexes immobilized on CNTs through π–π interactions.

3222 | *Inorg. Chem. Front.*, 2026, **13**, 3220–3236

This journal is © the Partner Organisations 2026

nected to a metal-complexing unit. As an example, Gouygou *et al.* have recently reported pyrene-tagged diphosphine ligands for the heterogenization of chiral rhodium complexes (Fig. 5b) on CNTs, applied to asymmetric hydrogenations.[33]

Pyrene has also been used as an anchoring group for dendritic units installed by Kim *et al.* on the surface of CNTs to accommodate metal salts (Au, Pt, and Ag) before reduction into metallic nanoparticles and further use as catalysts for nitroarene reduction.[34] The groups of Artero and Le Goff have also repeatedly used pyrene derivatization to immobilize electrocatalytic complexes of various metals, such as cobalt (tetraaza-macrocyclic Co complex),[35] nickel (Ni bisdiphosphine bioinspired complexes)[36,37] or copper[38,39] (Fig. 5c), on CNTs, and the constructs were applied to an array of energy-relevant transformations. In addition to chemically modified complexing units, some inherently aromatic metal complexes can be directly adsorbed on CNTs through $\pi$–$\pi$ interactions. For example, metal-containing porphyrins (Fig. 5d) have been assembled on CNTs for the development of electrochemical sensors, whereas rare-earth-complexing double-decker phthalocyanines were immobilized on CNTs with spintronic applications in mind.[40,41]

The main drawbacks of $\pi$–$\pi$ stacking arise from its relatively weak and reversible nature, which can compromise long-term stability and lead to the desorption of functional molecules under harsh conditions (*e.g.*, exposure to solvents, elevated temperatures, or electrochemical bias). Moreover, the limited control over molecular orientation and surface coverage may result in non-uniform functionalization and reduced reproducibility.

### Electrostatic interactions

Some other strategies exploit the charge characteristics of both CNTs and metal species, relying on the use of CNTs bearing charged groups (*e.g.*, carboxylates, sulfates, and amines) to attract and immobilize oppositely charged metal ions, clusters, or particles. This straightforward method permits rapid adsorption and can be tuned by adjusting the pH and ionic strength of the medium. The resulting assemblies could, however, suffer from limited stability in high ionic strength solutions due to charge masking, and a lack of selectivity in complex multi-ionic environments. To be fully effective, this approach requires a high density of charges that can be introduced, for example, by oxidative treatments of CNTs that lead to some damage of the nanotubes, which largely offsets the advantages of the non-covalent strategy. For instance, Mitra *et al.* reported the microwave-assisted oxidation of CNTs followed by their decoration with either Ag or Pt particles.[42] Although generating charges through chemical modification of carbon nanotubes is a common approach, it is also possible to use "native" ionic groups located in the sidewalls of carbon nanotubes, which originated from defects formed during CNT synthesis. Yet, this leads to poor decoration of the surface of the nanotube.

### Polymer wrapping

The immobilization of metal species can also be achieved by polymer wrapping around CNTs. This approach often leads to better dispersibility of the tubes and enables dense loading of metal species, offering tunable chemical functionality. However, uniform polymer coating of the CNT is mandatory to prepare adequate metal assemblies.

Many of the polymers employed are either polyaromatics or polyelectrolytes, aligning this strategy with those described above (*i.e.*, $\pi$–$\pi$ and electrostatic interactions). For example, Dong *et al.* reported the wrapping of CNTs with linear polyethyleneimine (LPEI, Fig. 6a), which was then used as a matrix to immobilize gold salts that were subsequently reduced into gold nanoparticles.[43] The approach neither required additional reducing agents nor involved extra oxidation of CNTs, beyond their initial purification step.

Bio-sourced polymers have also been used for the assembly of metal particles on CNTs. For example, chitosan was used both as a reducing agent of metal salts and as a stabilizing layer for the resulting NPs at the surface of nanotubes.[44]

Fluorene-based conjugated polymers (Fig. 6d and e) have been reported for the decoration of CNTs, relying mainly on $\pi$–$\pi$ interactions.[45] Depending on their molecular structure, these polymers were shown by the group of Nicholas to selectively interact with SWCNTs of specific diameters and chiralities.[46]

Other polymers can also interact with CNTs, allowing their coating. Among others, Lee *et al.* have reported polymer/CNT nanocomposites with enhanced electrical conductivity by non-covalently incorporating hydrophilic polymers such as polydopamine and poly(styrenesulfonate) to carbon nanotubes (Fig. 6c).[47]

### Hydrophobic effect/surfactants

Another possibility for the decoration of CNTs is to take advantage of the hydrophobic nature of their sidewalls to install lipid interfaces. In fact, amphiphilic lipids, combining a hydrophilic head group and hydrophobic hydrocarbon tail, can be assembled on CNTs thanks to the hydrophobic effect. This allows the adsorption of the lipophilic part of the lipids
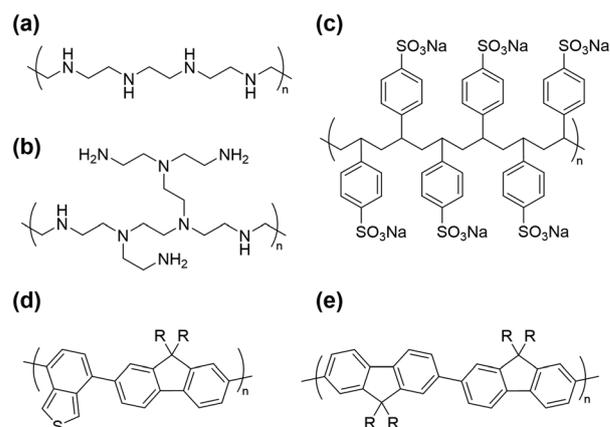


**Fig. 6** Examples of polymers reported for the decoration of CNTs: (a) linear and (b) branched polyethyleneimine; (c) polystyrene sulfonate; and (d–e) conjugated fluorene-based polymers.

on the CNT surface while their polar head groups are oriented towards the surrounding aqueous medium. Depending on the molecular structure of the amphiphiles, the decoration of the CNTs can be achieved with a variety of functional head groups, including ions, metal chelators or metal ligands. For instance, Li *et al.* have reported the use of cetyltrimethylammonium bromide, a cationic lipidic amphiphile, as a primary interface on CNTs to immobilize poly(sodium 4-styrenesulfonate) (PSS), which was then impregnated with iron(III) salts, precursors to magnetic $Fe_3O_4$ nanoparticles.[48] The immobilization of palladium NPs on CNTs was also carried out by Doris *et al.* through impregnation of lipid assemblies with Pd salts followed by their reduction into NPs under electron beam irradiation. The obtained structures were valorized in the electrocatalytic oxidation of ethanol in alkaline water.[49] In a more recent report, Lu *et al.* described the use of an amphiphilic glycopeptide for the decoration of carbon nanotubes and the *in situ* growth of palladium particles.[50] In this example, the hydrophobic peptide region was rich in phenylalanine, an aromatic amino acid, strengthening the anchoring of the molecule on the tube's surface through $\pi$–$\pi$ interactions in addition to the hydrophobic effect. The assembly was then employed as a catalyst for the reduction of 4-nitrophenol into the corresponding 4-aminophenol, using near infrared illumination to increase the temperature of the mixture and accelerate the reaction.

The lipid interface strategy can be applied to virtually any type of CNT, regardless of their surface state. However, drawbacks such as incomplete covering of the CNT surface or instability of the lipid assembly under different stress conditions (solvent, temperature, and pH) limit the scope of this strategy. With these shortcomings in mind, our group has developed an approach that relies on nanoring-forming photopolymerizable amphiphilic molecules, leading to stable lipid assemblies at the surface of CNTs. The latter approach combines both the advantages of non-covalent functionalization (preservation of the structural integrity of the CNTs) and of the covalent functionalization (robustness of the supra-molecular assembly on CNTs). This variant of polymerized lipid interfaces for the functionalization of CNTs will be detailed in the following section.

## Self-assembled polymerized lipid interfaces to immobilize metals on CNTs

Early findings concerning the aqueous organization of surfactants around carbon nanotubes demonstrated the ability of some amphiphilic lipids to form hemi-cylindrical micelles on the carbonaceous matrix.[51] This structuration is driven by the hydrophobic effect that holds the lipidic tails of the amphiphiles in contact with the tube's surface while their polar head groups are oriented towards the surrounding aqueous medium. The resulting ring-shaped self-assemblies can adopt different orientations, depending on the tube type and the molecular structure of the surfactant, but are usually oriented perpendicular to the tube's axis. Interestingly, nano-rings can

be formed on different types of CNTs and afford dense and homogeneous decoration with lipids that can incorporate different functionalities. Unfortunately, the strategy is undermined by the fragility of the supramolecular structures. Indeed, they can break down under various conditions, for example in the presence of organic solvents, at high temperatures, or in response to changes in the salinity of the medium.

In this context, our group has developed a strategy to decorate multi-walled CNTs with robust ring-like lipidic structures, relying on the use of diacetylene-containing amphiphilic units as building blocks. In fact, diacetylenes can undergo polymerization upon light activation, triggering a topochemical 1,4-addition reaction between diacetylene monomers to form a conjugated polydiacetylene backbone. In water, these diacetylene amphiphiles initially self-assemble into spherical micelles (Fig. 7a). When nanotubes are added, a new hydrophobic component is introduced to the mixture (Fig. 7b), and micelles rearrange into hemi-micellar nanorings on the surface of the CNTs upon ultrasonication (Fig. 7c). The nanorings can then be photopolymerized under illumination at 254 nm (Fig. 7d). UV irradiation triggers the topochemical 1,4-addition of diacetylene units between neighboring amphiphiles (Fig. 7d, inset), leading to the formation of ene–yne conjugated networks within the core of each individual nanoring. Notably, the rings are simply reinforced thanks to the topochemical process, without any covalent bonding with the graphitic surface of the CNTs. After the polymerization step, the rings become much more stable and remain attached to the CNT, even under drastic conditions such as ethanol washings,
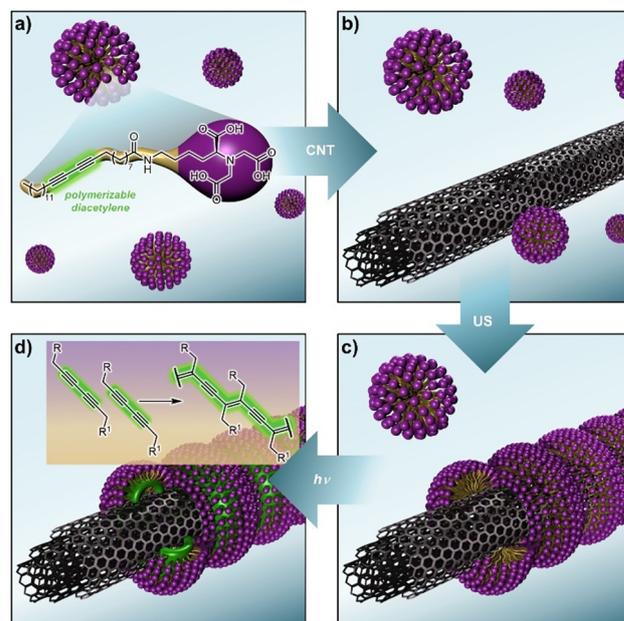


**Fig. 7** Decoration of MWCNTs with polymerized nanorings: (a) micelle colloid with an example of a diacetylene amphiphile (*i.e.,* DANTA); (b) introduction of nanotubes in the mixture; (c) rearrangement of micelles into nanorings upon sonication; (d) stabilization of the rings by photopolymerization under UV light.

dialysis, high temperatures, *etc*. The structure of the main amphiphilic unit that we have developed for the coating of CNTs and photo-polymerization is illustrated in Fig. 7a. At the end of the process, nanotubes are recovered with an anionic surface because of the presence of the carboxylate head groups from the starting amphiphiles. The polymerized rings can be used to directly anchor metallic species, albeit with low efficiency, or serve as a primary organic interface in a multi-layered hybrid architecture. To achieve this multi-layer assembly, a second coating is deposited on the anionic surface in the form of a polycationic polymer. The latter is maintained by multiple electrostatic interactions and will serve as a 3D environment suitable for the robust immobilization and stabilization of metallic nanoparticles.

When it comes to the preparation of catalytic materials, this type of assembly offers three key advantages over known heterogeneous systems, *i.e.*, (i) the presence of a lipophilic domain (lipid core of the nanorings) that could behave as a nano-reactor combined with (ii) the close vicinity of the active catalytic species, and (iii) the ease of recycling thanks to the CNT support.

## Immobilization of metal nanoparticles for catalytic applications

As mentioned above, amphiphiles containing a diacetylene (DA) function and a nitrilotriacetic (NTA) headgroup (see the structure of DANTA, Fig. 8a) were used for the formation of a polymerized nanoring (pDANTA) forming a primary organic layer and affording dense coverage of the CNTs with negative charges. A secondary organic layer, composed of a cationic polymer, namely poly(diallyldimethylammonium chloride) (PDADMAC), was then deposited through electrostatic interactions (Fig. 8b), providing a three-dimensional network suitable for the stabilization and attachment of pre-formed metal particles (Fig. 8c). This approach leads to the homogeneous coverage of the CNT surface with metal nanoparticles, taking full advantage of the high specific surface area of the carbonaceous material (Fig. 8d). The multitude of interconnected ammonium groups enables robust immobilization of NPs on the surface of the CNT, and nanoparticles' stabilization occurs through the so-called "electro–steric" interactions[52] with the ammonium cations of PDADMAC, mediated by both electrostatic and steric effects. Each quaternary ammonium cation forms a rather weak bond with the metal surface, thus providing good accessibility to the reagents to be converted during the catalytic transformation.

Over the years, these features of the metal–CNT hybrids were exploited by us for the promotion of a variety of chemical transformations. Depending on the foreseen application, various metal species have been immobilized on CNTs through the nanoring-based layer-by-layer strategy.

**Gold particles.** The first construction that was studied in our group resulted from the layer-by-layer assembly of gold nanoparticles on carbon nanotubes. The hybrid was obtained by first sonicating CNTs in the presence of an aqueous colloid of diacetylene amphiphiles to form nanorings that were subsequently polymerized under UV illumination. The polyammonium layer was then deposited and finally, pre-formed THPC-reduced AuNPs were added, giving rise to the hybrid (AuCNT) as an aqueous suspension. Gold content was measured by inductively coupled plasma mass spectroscopy (ICP-MS) techniques after mineralization.

The gold assembly was valorized in a variety of chemical processes, starting with the aerobic oxidation of silanes into silanols (Fig. 9). The transformation was easily carried out by simply mixing the silane substrate and the catalyst (0.1 mol%) in THF, under air and at room temperature.

The catalytic system could easily oxidize both alkyl and aryl silanes in very good yields, with no siloxane by-product, and was found to be recyclable without any loss of catalytic activity
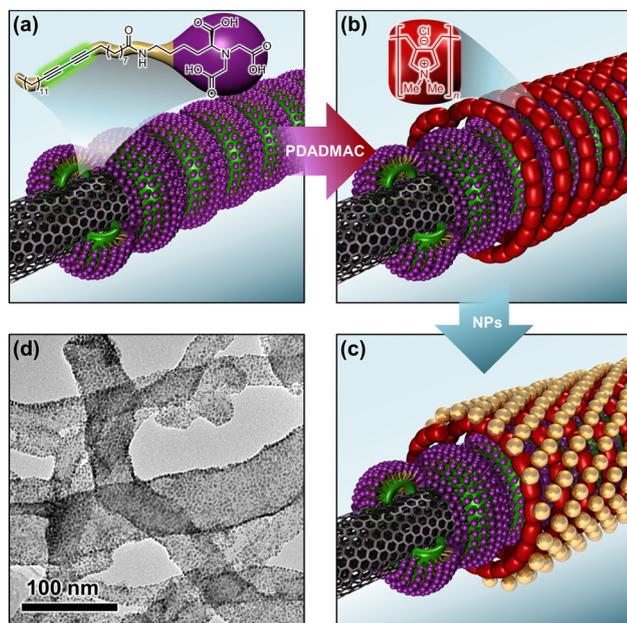


**Fig. 8** Decoration of MWCNTS with metal particles: (a) polymerized nanorings; (b) electrostatic deposition of the secondary organic layer with the chemical structure of PDADMAC; (c) immobilization of pre-formed metal particles; and (d) an example of a TEM micrograph of the final assembly (AuCNT).
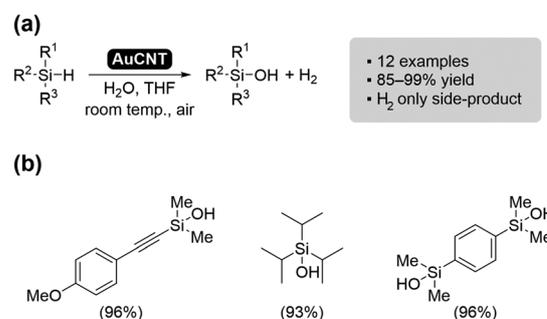


**Fig. 9** Aerobic oxidation of silanes with AuCNTs: (a) overview of the process and (b) selected examples of obtained products.

This journal is © the Partner Organisations 2026

*Inorg. Chem. Front.*, 2026, **13**, 3220–3236 | **3225**

over numerous cycles.[53] It was also operational with minute amounts of catalyst, down to 0.001 mol%, and showed an excellent turnover number (TON = 72 000) and turnover frequency (TOF = 12 000 h$^{-1}$). Furthermore, it was demonstrated that both water and oxygen were needed for the reaction to proceed, and that the OH group of silanol originated from water. Interestingly, the silane oxidation process gave rise to one equivalent of hydrogen gas as the only side-product of the reaction. This prompted the exploration of the use of the AuCNT hybrid combined with a sacrificial silane in the promotion of hydrogenative transformations, such as the direct reductive amination of aldehydes (Fig. 10).[54] In this transformation, gold plays a dual role: (i) it acts as a Lewis acid to promote the condensation of the aldehyde with the amine, and (ii) it activates the silane to enable the reduction of the formed imine into a silylated amine which is then hydrolyzed *in situ* to the desired secondary amine. The process proved highly efficient on a variety of aldehydes operating in water, under air, with minimal catalyst loading, and showed good recyclability. The association of a silane with the AuCNT hybrid was also found to diligently catalyze the reduction of diverse aromatic and aliphatic amine *N*-oxides. The methodology was operative at room temperature, with low catalytic loading (0.4 mol%), good recyclability and a wide array of *N*-oxides.[55]

The CNT-supported gold nanohybrid was likewise exploited for the aerobic oxidation of alcohols under mild conditions, requiring neither added O$_2$ nor heating (Fig. 11a). The process mainly provided chemoselective oxidation of alcohols and aldehydes to the corresponding acids when reactions were conducted in a mixture of toluene/water. Interestingly, under anhydrous conditions, aldehydes could be selectively obtained from primary alcohols.[56] When carried out in methanol, the aerobic oxidation of alcohols, and that of aldehydes, with the AuCNT catalyst yielded methyl esters (Fig. 11b). The system operated under sustainable conditions, namely low catalytic loading (0.1 mol%), room temperature and atmospheric pressure of air, with the possibility of recycling the CNT-supported gold catalyst.[57]

In another study, the AuCNT system was studied for the room temperature oxidation of phenol-related substrates
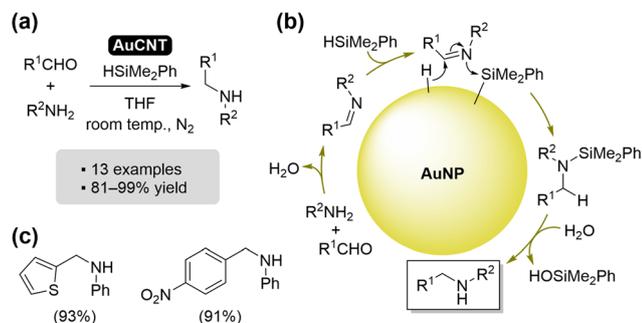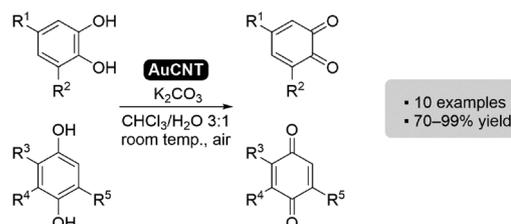


**Fig. 10** Reductive amination of aldehyde AuCNTs and HSi(Me)$_2$Ph: (a) overview of the process; (b) proposed mechanism; and (c) selected examples of obtained products.
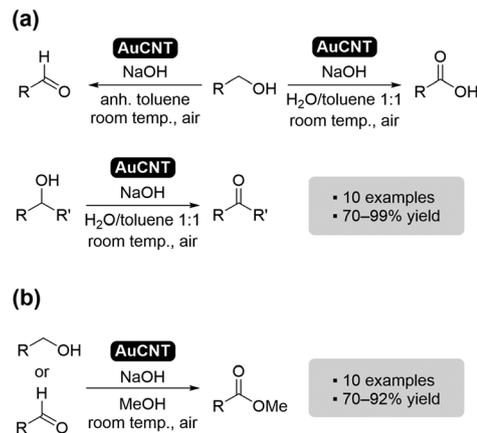


**Fig. 11** (a) Overview of the AuCNT-catalyzed alcohol oxidation process. (b) Overview of the conversion of alcohols or aldehydes to methyl esters with AuCNTs.

(Fig. 12), such as hydroquinones, catechols, aminophenols or thiols. It operated under air atmosphere with no external oxidant, was easily recycled, and was efficient even in modest amounts (down to 0.013 mol% of gold).[58] The ability of the AuCNT hybrid to oxidize catechols motivated the use of a related catalyst in processes that mimic metalloenzymes.[59]

The size of nanoparticles supported on carbon nanotubes was shown to influence the catalytic behavior of AuCNT systems assembled with either 3 nm or 20 nm gold nanoparticles. Although both small and large nanoparticles efficiently catalyzed silane oxidation, alcohol oxidation, reductive amination, and hydroquinone oxidation, activities normalized to the total gold content consistently yielded higher turnover frequencies for the smaller particles. However, when catalytic activity was normalized to the number of surface gold atoms, the size effect became much less pronounced for most reactions. The fraction of surface atoms (or dispersion, $D$) can be estimated using the relationship $D = 0.9/d$, where $d$ is the particle diameter in nanometers. This provides a good approximation for spherical gold nanoparticles. In simpler terms, the fraction of exposed metal atoms is inversely proportional to particle size: a 1 nm particle exposes nearly all its atoms, whereas a 2 nm particle exposes approximately 45% of its atoms, and this fraction decreases further as particle size increases. Therefore, sites involved in the catalytic transformations are only those directly exposed to the medium.[60]



**Fig. 12** Overview of the oxidation of phenol derivatives with AuCNTs.

**3226** | *Inorg. Chem. Front.*, 2026, **13**, 3220–3236

This journal is © the Partner Organisations 2026

Using the AuCNT along with aqueous formaldehyde, the N-formylation of amines was investigated (Fig. 13). The transformation was effective under air atmosphere, at room temperature, with excellent chemoselectivity and recyclability.[61]

Additional work showed that benzoins or benzhydrols could be oxidized and condensed with aromatic 1,2-diamines to yield quinoxalines using AuCNTs as a recyclable heterogeneous catalyst (Fig. 14a). The transformation proceeded in one-pot with excellent yield, under air and at room temperature.[62] Other oxidative applications of the AuCNT catalyst were investigated, such as the oxidation of hydroxylamines[63] (Fig. 14b) or 1,4-dihydropyridines (Fig. 14c).[64]

The conversion of thioamides into their nitrile counterparts was also promoted with a low amount of AuCNTs (0.35 mol%),
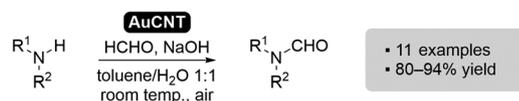


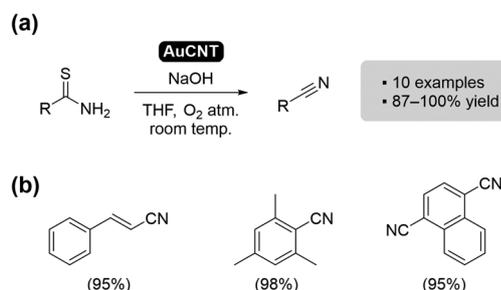**Fig. 13** N-Formylation of amines with AuCNTs.



**Fig. 15** (a) Overview of the AuCNT-catalyzed thioamide to nitrile transformation and (b) selected examples of obtained products.
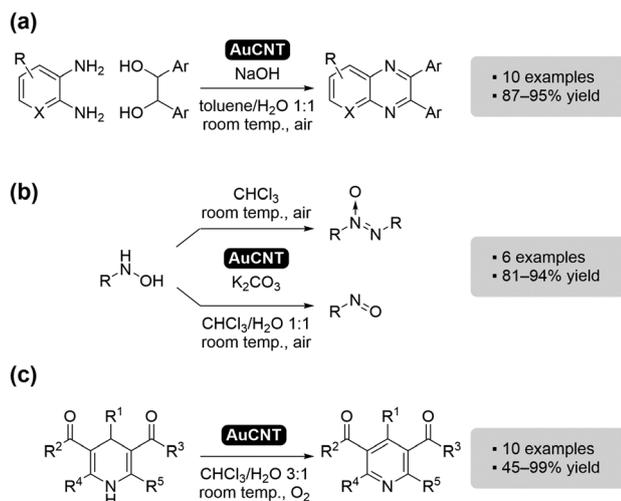


**Fig. 14** Various oxidative transformations promoted by the AuCNT hybrid: (a) formation of quinoxalines from aromatic 1,2-diamines; (b) oxidation of hydroxylamines; and (c) oxidation of 1,4-dihydropyridines.

under an oxygen atmosphere (Fig. 15). The process proved efficient on a variety of substrates and the catalyst could be recovered and reused in subsequent reactions.[65]

Apart from numerous organic transformations, the AuCNT hybrid was used for the promotion of energy-related reactions. For instance, it was shown to be an electrochemically active catalyst, after deposition on glassy carbon, for the oxygen reduction reaction,[66] a key transformation in fuel cells and $O_2$ sensors. The AuCNT hybrid was active in acidic media, but its performances were particularly striking in alkaline media, rivaling the performances of Pt-based materials under such conditions. AuCNTs also proved to be a promising material for selective electroreduction of $CO_2$ to CO under aqueous conditions after deposition on a gas diffusion layer (GDL) electrode.[67] For the latter transformation, a very small amount of gold resulted in high current density (10 mA cm$^{-2}$ at −0.55 V vs. SHE) in water, highlighting a remarkably high mass activity of the assembly.

In addition to providing solid support, CNTs can form entangled aggregates, thanks to their fibrillar morphology. This property can be leveraged to immobilize the assemblies within the restriction zone of a specifically designed microfluidic chip (Fig. 16). Such a strategy was employed to prepare continuous flow catalytic systems that were applied to both organic transformations (oxidation of silanes)[68] and photocatalytic processes (hydrogen photo-production).[69] Several benefits over conventional batch transformations were thus obtained, such as continuous production, ease of use, reusability, reaction control and safety.

**Palladium particles.** A layer-by-layer coating of the nanotube, identical to that used for the immobilization of gold NPs, was employed to immobilize NaBH$_4$-reduced Pd nanoparticles on CNTs. This allowed the preparation of CNTs densely covered with Pd nanoparticles which, based on transmission electron microscopy, were of a spherical shape and had an average diameter of ca. 2 nm. The particles were found to be composed of both palladium metal and palladium oxide in a 1:1 ratio, as determined by X-ray photoelectron spectroscopy (XPS) analysis.

The Pd-based architecture (PdCNT) was valorized in the Suzuki cross-coupling reaction under sustainable conditions (Fig. 17).[70] The PdCNT hybrid was studied for the promotion of the transformation in an EtOH/water mixture, at room
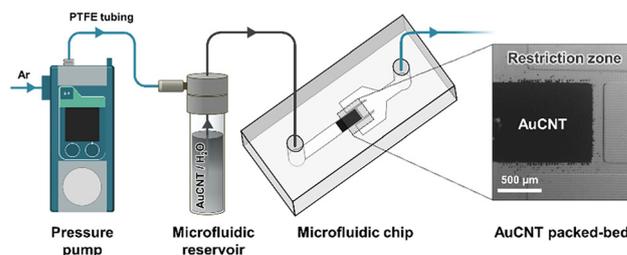


**Fig. 16** Schematic representation of the preparation of an AuCNT packed bed in a microfluidic chip.

This journal is © the Partner Organisations 2026

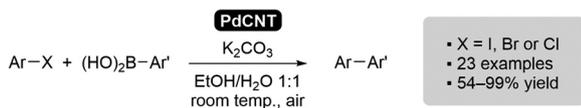Inorg. Chem. Front., 2026, **13**, 3220–3236 | **3227**

**Fig. 17** Overview of the Suzuki coupling reaction promoted by PdCNT.

temperature, in an open flask, and proved efficient on a variety of substrates. It is worth mentioning that this was the first example of a heterogeneous system able to catalyze the Suzuki coupling of aryl chlorides without the need for thermal activation.

The PdCNT nanohybrid was employed along with cuprous chloride in the co-catalytic Tsuji–Wacker oxidation of olefins (Fig. 18). The system tolerated various functional groups and demonstrated high selectivity, leading preferentially to the formation of methylketone derivatives. Moreover, it required minimal amounts of the co-catalysts to operate at room temperature and proved readily recyclable.[71]

PdCNTs were also later used in the C–H arylation of quinone derivatives. Interestingly, C–H activation was achieved using only 0.1 mol% of palladium, whereas 10 mol% of Pd was required under homogeneous conditions.[72]

**Platinum particles.** The nanotube platform was also used for the immobilization of platinum nanoparticles. Characterization by electronic microscopy showed uniform decoration of the CNT surface with small spherical Pt nanoparticles (2.1 nm average diameter). Pt(0) was the main species together with some higher oxidation state derivatives (Pt(II) and Pt(IV), mostly), as examined by XPS.

The platinum-based catalyst was used in the anti-Markovnikov hydrosilylation of alkenes and alkynes under solvent-free conditions (Fig. 19). The system showed excellent
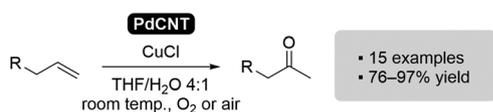
results on a wide scope of alkenes/alkynes, even on complex structures, operated under sustainable conditions (room temperature, 0.04 mol% catalyst loading, and air atmosphere) and allowed for recycling and reuse of the nanohybrid with no alteration of its performances.[73]

**Ruthenium particles.** In a similar fashion, ruthenium nanoparticles of 2 nm were immobilized on CNTs through the lipid nanoring strategy, leading to the RuCNT hybrid. The latter was used in the hydrazine-mediated catalytic hydrogenation of nitroarenes, at room temperature. Excellent selectivity was observed, both for the substrate (only the nitro groups were converted) and for the reaction product. In fact, the catalyst could selectively convert nitroarenes into the corresponding anilines when the reaction was carried out in water, whereas it provided exclusively the corresponding N-aryl hydroxylamines when the same reaction was run in THF (Fig. 20a). Regardless of the solvent used, the catalyst could be recycled and reused for more than five cycles.[74] Building on the results of the previous work, 2-nitrochalcones were converted to quinoline N-oxides at room temperature (Fig. 20b). The RuCNT catalyst allowed the one-pot reduction–condensation sequence to take place under mild and sustainable conditions.[75]

A mild oxidation method to prepare sulfones from sulfides was developed using RuCNTs in combination with sodium periodate. The system proved efficient for the oxidation of a variety of substrates and permitted the preparation of compounds with potential biological activity in a simple and versatile way (Fig. 21).[76]

**Rhodium particles.** Robust anchoring of small (2 nm) rhodium nanoparticles on CNTs could also be achieved by the nanoring-based approach. The resulting RhCNT construct was valorized for the dehydrogenation of secondary amines, including various N-heterocycles of synthetic interest (Fig. 22c). The latter system was designed to mimic metalloenzymes that operate thanks to a metal center coupled with a quinone cofactor. Thus, the Rh-based hybrid served as a co-catalyst (1 mol%), along with tert-butylcatechol (10 mol%), in a bioinspired process that operated through an addition–elimination pathway (Fig. 22b). The co-catalytic system was active under mild conditions (ambient atmosphere and room temp-



**Fig. 18** Overview of the Tsuji–Wacker oxidation of olefins catalyzed by the PdCNT hybrid.



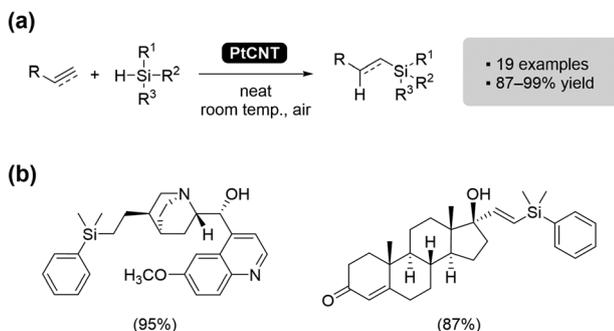**Fig. 19** (a) Overview of the PtCNT-catalyzed hydrosilylation of alkenes and alkynes and (b) selected examples of obtained products.
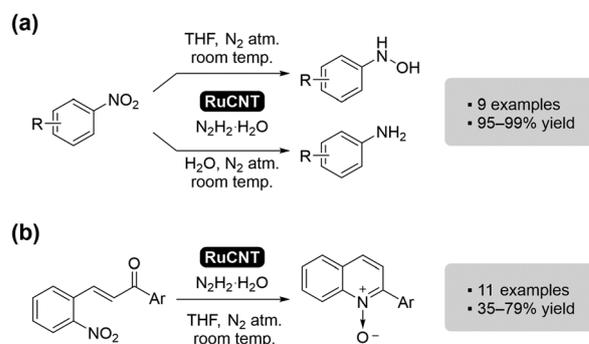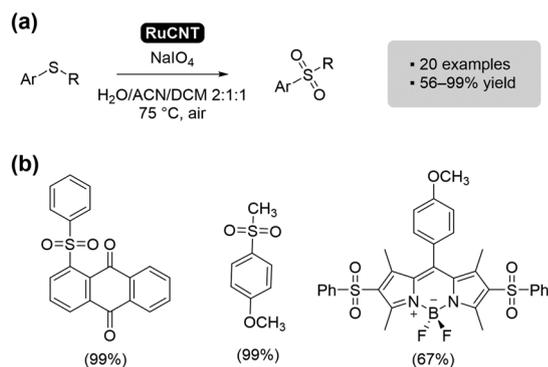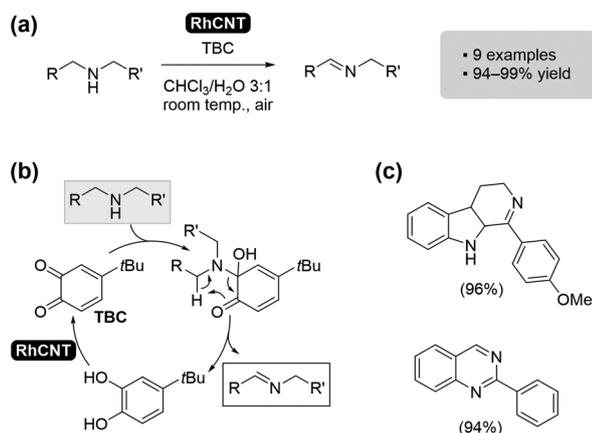


**Fig. 20** Hydrazine-mediated processes using RuCNTs: (a) hydrogenation of nitroarenes and (b) conversion of 2-nitrochalcones to quinoline N-oxides.

**3228** | *Inorg. Chem. Front.*, 2026, **13**, 3220–3236

This journal is © the Partner Organisations 2026

**Fig. 21** (a) Overview of the RuCNT-catalyzed sulfide oxidation and (b) selected examples of obtained products.
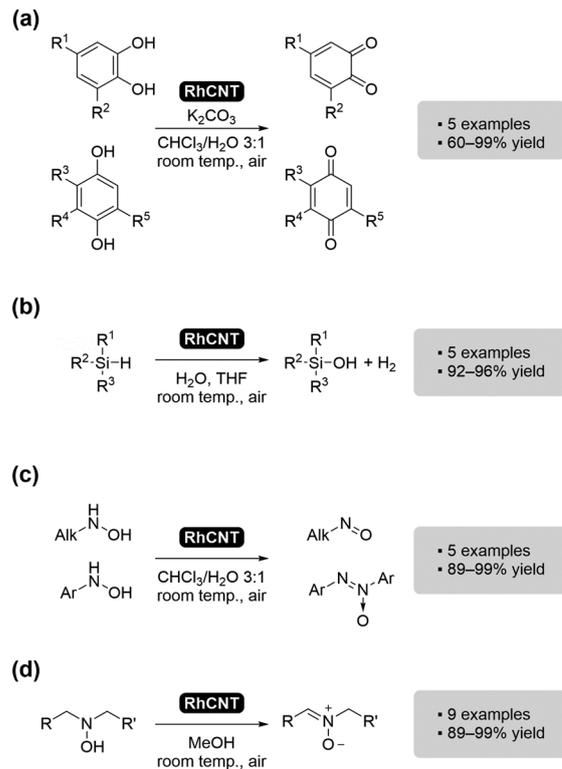


**Fig. 22** (a) Overview of the co-catalytic dehydrogenation of N-heterocycles using *tert*-butylcatechol (TBC) and RhCNTs; (b) putative addition–elimination mechanism; and (c) selected examples of obtained products.



**Fig. 23** Various oxidative processes catalyzed by the RhCNT hybrid: (a) oxidation of hydroquinones; (b) oxidation of silanes; (c) oxidation of hydroxylamines; and (d) oxidation of hydroxylamines to nitrones.

erature) and promoted the dehydrogenation of secondary amine-containing substrates, giving access to scaffolds such as indoles, carbazoles, acridines, quinolines, dihydroisoquinolines, and dihydro-β-carbolines.[77]

The usefulness of the carbon nanotube–rhodium hybrid was further demonstrated through the oxidation of different organic substrates.[78] At room temperature and with low RhCNT loading, hydroquinones (Fig. 23a), silanes (Fig. 23b), hydroxylamines (Fig. 23c and d),[79] hydrazines, and thiols were efficiently and selectively oxidized. Furthermore, RhCNT was combined with aryl diselenides/hydrogen peroxide for the co-catalytic oxidation of naphthols, leading to benzenoid A-ring-functionalized quinones.[80]

**Bi-metallic particles – ruthenium–rhodium.** A bimetallic hybrid was prepared through the same layer-by-layer strategy but, in that case, the nanoparticles were obtained from the co-reduction of a 1 : 1 mixture of Ru and Rh salts before their deposition on the CNT platform. TEM analysis of the resulting hybrid (RuRhCNTs) showed objects very similar to individual RuCNTs or RhCNTs, with small spherical particles evenly dis-

tributed all over the CNT surface. However, elemental mapping was performed by energy dispersive X-ray spectroscopy (EDS) to gain further insight into metal distribution at the surface of the nanotubes (Fig. 24). Well-separated high energy K-lines of Ru and Rh enabled discrimination and showed that the two metals were blended/alloyed with a 57 : 43
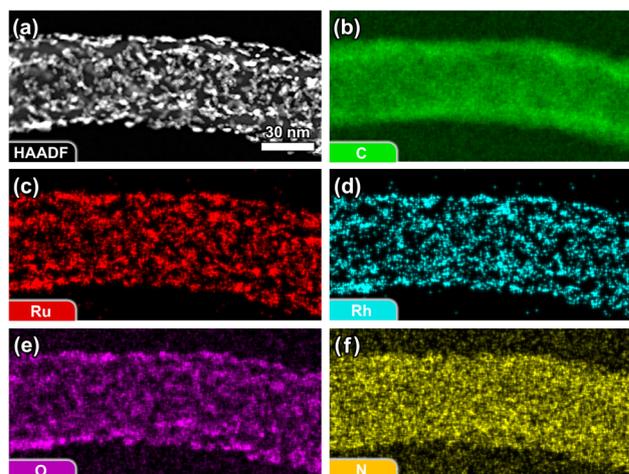


**Fig. 24** (a) High angle annular dark field (HAADF) image of the RuRhCNT hybrid and associated EDS mapping for (b) carbon; (c) ruthenium; (d) rhodium; (e) oxygen; and (f) nitrogen.

This journal is © the Partner Organisations 2026

*Inorg. Chem. Front.*, 2026, **13**, 3220–3236 | **3229**

Ru/Rh ratio. Through XPS analysis, Ru(0) and Rh(0) were identified as the main species present in the nanoparticles together with some higher oxidation state derivatives, *i.e.* Ru(IV) and Rh(IV).

The RuRhCNT hybrid was used to functionalize alkenes and alkynes through different reactions (Fig. 25), namely hydrothiolation,[81] hydrophosphinylation[82] and hydroboration.[83] In all cases, the system proved to be efficient under mild and sustainable conditions (0.04 mol% catalyst loading, room temperature), for a variety of structurally different substrates, and could be recycled without any significant loss of activity. The association of rhodium with ruthenium permitted a synergistic effect, resulting in a system that was more efficient than those based on the monometallic RhCNT and RuCNT hybrids, used either individually or in combination.

**Base metal particles.** The utility of the polymerized lipid-based interface strategy is not limited to the immobilization of noble metal particles. In fact, the method has been applied to the anchoring of different ferrite particles. For instance, copper ferrite nanoparticles of a spherical shape with an average diameter of 4.8 nm were assembled on multiwalled CNTs and their binary nature was confirmed by XPS (based on Cu 2p and Fe 2p regions).

The CuFe$_2$O$_4$CNT hybrid was then used for the promotion of the 1,3-dipolar cycloaddition of alkynes with *in situ* generated organic azides (Fig. 26a).[84] CuFe$_2$O$_4$CNTs offered key features, such as operation in aqueous solvent, low catalytic loading, room temperature, air atmosphere, and magnetic recovery (Fig. 26e) to facilitate separation from the reaction mixture before recycling. The hybrid was further used as a catalyst for the borylation of unsaturated C–C bonds (Fig. 26b)[85] as well as for the efficient A-ring selenation of naphthoquinones and anthraquinones to gain access to new potent trypanocidal compounds (Fig. 26c and d).[86]

CNTs were also decorated with nickel(II) hydroxide particles through a similar layer-by-layer strategy. Interestingly, microscopic analysis showed that the small spherical nanoparticles
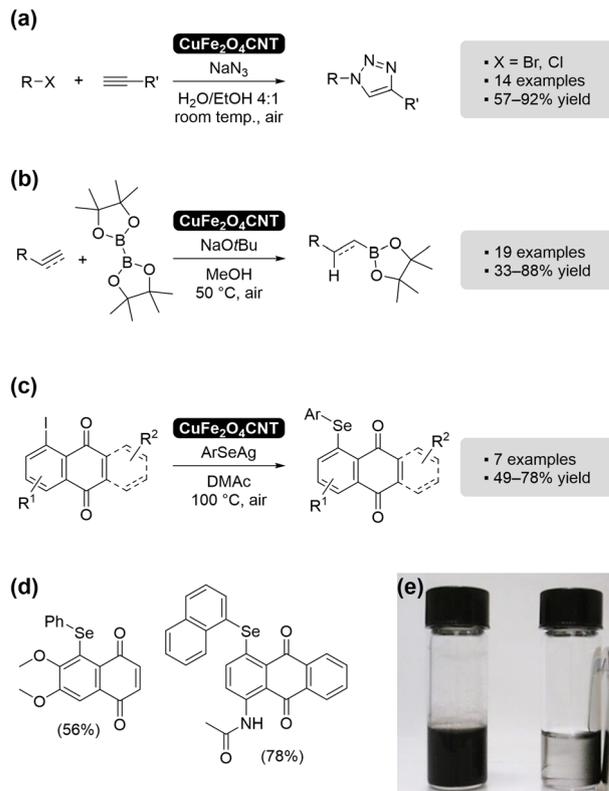
**Fig. 26** Transformations using CuFe$_2$O$_4$CNT as a catalyst: (a) 1,3-dipolar cycloaddition of alkynes with *in situ* generated azides; (b) borylation of alkenes and alkynes; and (c) A-ring selenation of naphthoquinones. (d) Examples of selenated quinone products. (e) Application of a permanent magnet for easy recovery of the catalyst.

observed when the sample was kept in THF (Fig. 27a) transformed into a continuous porous film when the assembly was transferred into water (Fig. 27b). XPS analysis indicated that, despite the morphological evolution, no alteration of the oxidation state of Ni had occurred, confirming the Ni(OH)$_2$
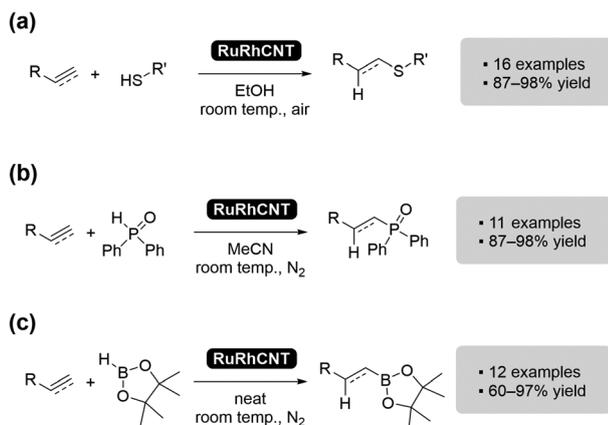
**Fig. 25** RuRhCNT-catalyzed processes for the functionalization of alkenes and alkynes: (a) hydrothiolation; (b) hydrophosphinylation; and (c) hydroboration.
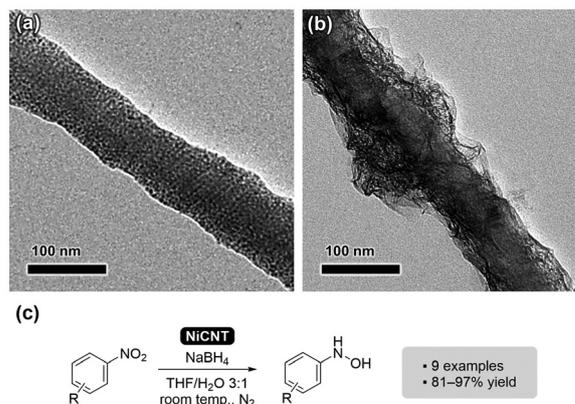
**Fig. 27** TEM micrographs of the NiCNT hybrid in (a) THF and (b) water. (c) Overview of the borohydride-mediated selective reduction of nitroaromatics using NiCNT as a catalyst.

3230 | *Inorg. Chem. Front.*, 2026, **13**, 3220–3236

This journal is © the Partner Organisations 2026

nature of both the nanoparticles and film. This construction proved very efficient in the borohydride-mediated selective reduction of a variety of nitroaromatics, under mild conditions (Fig. 27c).[87]
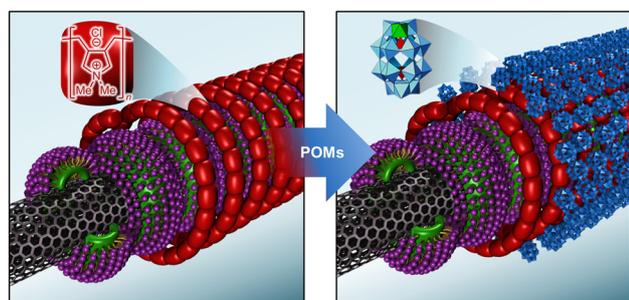
## Immobilization of miscellaneous metal species

Even though the nanoring-based lipid interface strategy has been mainly exploited for the assembly of metal particles, it can also be employed to immobilize discrete molecular structures at the surface of CNTs.

Tungsten-based polyoxometalates (POMs) with varying numbers of nickel centers were synthesized and immobilized on CNTs, following the layer-by-layer procedure (Fig. 28). POMs are anionic molecular metal oxides based on early, high-valent transition metals,[88] and their negative charge enables strong interactions with polycations such as PDADMAC (the secondary organic layer deposited on nanorings).
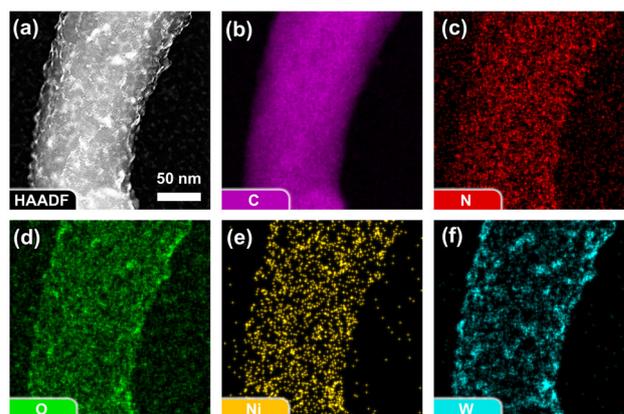
The morphology of the POMCNT assemblies was investigated by scanning transmission electron microscopy (STEM) using high angle annular dark field (HAADF) imaging. In parallel, EDS allowed the mapping of C, W, and Ni elements present in the hybrids, showing that POMs were regularly and densely distributed on CNTs (Fig. 29).

Electrochemical investigations on the POMCNT-promoted hydrogen evolution reaction (HER) highlighted the benefits of heterogenization in terms of electro-catalytic activity. In fact, lower onset potentials and higher current densities were observed for immobilized POMs compared to their free-standing counterparts.[89]

In another study, the nanoring-based lipid interface strategy was applied to the immobilization of cobaloximes on CNTs. To this end, a specific amphiphile (DAPy), composed of a diacetylene-containing lipid tail and a pyridine head group, was designed and synthesized. The rationale behind this structure was to take advantage of the inherent affinity of pyridines as axial ligands of cobaloximes.[90] In acidic aqueous medium, DAPy became protonated (formation of pyridiniums) and, in the presence of CNTs, self-assembled at their surface (Fig. 30a). This self-assembly gave rise to nanoring structures covering the surface of the nanotube, that were polymerized



**Fig. 29** (a) High angle annular dark field (HAADF) image of the POMCNT hybrid and associated EDS mapping for (b) carbon; (c) nitrogen; (d) oxygen; (e) nickel; and (f) tungsten.
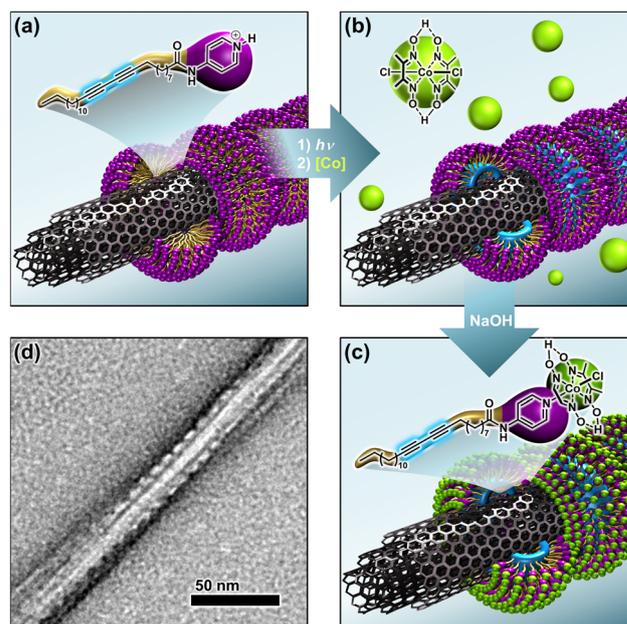


**Fig. 30** Heterogenization of cobaloximes on carbon nanotubes: (a) formation of DAPy nanorings on MWCNTs; (b) polymerization of the rings and addition of cobalt species; (c) alkalinization of the medium and immobilization of cobalt complexes; and (d) TEM micrograph of the hybrid showing ring-shaped structures at the surface of the nanotubes.

under UV light (Fig. 30b). This afforded a uniform coverage of the CNT surface with pyridine anchoring groups. After alkalinization of the medium, the pyridinium head groups were neutralized and made available for coordination to cobalt complexes, so that the addition of cobaloximes yielded the final CNT–pDAPy–Co nanohybrid (Fig. 30c).

TEM showed a homogeneous distribution of lipid nanorings oriented perpendicular to the axis of the nanotubes (Fig. 30d). XPS analysis confirmed the presence of cobaloximes at the surface of the nanohybrid and permitted the assessment



**Fig. 28** Immobilization of POMs on carbon nanotubes through electrostatic interactions using the nanoring-based layer-by-layer strategy.

This journal is © the Partner Organisations 2026

*Inorg. Chem. Front.*, 2026, **13**, 3220–3236 | **3231**

**Table 1** Overview of the hybrid catalysts prepared through the polymerized nanoring-based strategy

| Hybrid | Metal species | Immobilization | Transformations | Performance metrics | Durability/stability | Leaching | Ref. |
|---|---|---|---|---|---|---|---|
| AuCNTs | Au particles of ca. 3 nm (reduction of HAuCl$_4$ using THPC/NaOH) | Electro-steric interactions | Silane oxidation | TON = 72 000; TOF = 12 000 h$^{-1}$ | Stable over 5 cycles | ND (ICP-MS) | 53 |
| | | | Reductive amination | TON = 21 250; TOF = 1328 h$^{-1}$ | Stable over 5 cycles | ND (SF) | 54 |
| | | | Deoxygenation of amine N-oxides | TON = 1300; TOF = 54 h$^{-1}$ | Stable over 5 cycles | ND (SF) | 55 |
| | | | Alcohol oxidation | TON = 495; TOF = 165 h$^{-1}$ | Stable over 3 cycles | ND (SF) | 56 |
| | | | Alcohols into esters | TON = 620; TOF = 3 h$^{-1}$ | Stable over 3 cycles | ND (ICP-MS) | 57 |
| | | | Oxidation of phenols | TON = 4217; TOF = 263 h$^{-1}$ | Stable over 5 cycles | ND (SF) | 58 |
| | | | N-Formylation of amines | TON = 512; TOF = 17 h$^{-1}$ | Stable over 5 cycles | ND (SF) | 61 |
| | | | Quinoxaline synthesis | TON = 480; TOF = 18 h$^{-1}$ | Stable over 5 cycles | ND (SF) | 62 |
| | | | Aromatization of 1,4-dihydropyridines | TON = 982; TOF = 18 h$^{-1}$ | Stable over 5 cycles | NT | 64 |
| | | | Dehydrosulfurization of thioamides | TON = 2629, TOF = 876 h$^{-1}$ | Stable over 5 cycles | NT | 65 |
| | | | O$_2$ reduction reaction | 0.98 V vs. RHE onset 250 mV overpotential | Stable ORR at 0.6 V vs RHE over 15 h | NT | 66 |
| | | | CO$_2$ reduction reaction | 10 mA cm$^{-2}$ at $-0.55$ V vs. SHE | Stable CO production (0.52 µmol s$^{-1}$) over 4 h | NT | 67 |
| PdCNTs | Pd particles of ca. 2 nm (reduction of [PdCl$_2$(CH$_3$CN)$_2$] using LiEt$_3$BH) | Electro-steric interactions | Suzuki coupling | TON = 408; TOF = 20 h$^{-1}$ | Stable over 5 cycles | ND (SF) | 70 |
| | | | Tsuji–Wacker oxidation | TON = 830; TOF = 7 h$^{-1}$ | Stable over 5 cycles | ND (SF) | 71 |
| | | | C–H arylation of quinones | TON = 3002; TOF = 44 h$^{-1}$ | Stable over 3 cycles | NT | 72 |
| PtCNTs | Pt particles of ca. 2 nm (reduction of H$_2$PtCl$_6$·6H$_2$O by heating at 160 °C in ethylene glycol/NaOH) | Electro-steric interactions | Hydrosilylation of alkenes/alkynes | TON = 14 525; TOF = 102 h$^{-1}$ | Stable over 6 cycles | ND (SF, ICP-MS) | 73 |
| RuCNTs | Ru particles of ca. 2 nm (reduction of RuCl$_3$·6H$_2$O by heating at 160 °C in ethylene glycol/NaOH) | Electro-steric interactions | Nitroarene reduction | TON = 4150; TOF = 830 h$^{-1}$ | Stable over 5 cycles | ND (SF) | 74 |
| | | | Reduction of 2-nitrochalcones | TON = 720; TOF = 360 h$^{-1}$ | Stable over 5 cycles | ND (ICP-MS) | 75 |
| | | | Oxidation of sulfides | TON = 5000; TOF = 1000 h$^{-1}$ | Stable over 5 cycles | NT | 76 |
| RhCNTs | Rh particles of ca. 2 nm (reduction of RhCl$_3$·3H$_2$O by heating at 160 °C in ethylene glycol/NaOH) | Electro-steric interactions | Dehydrogenation of N-heterocycles | TON = 470; TOF = 9 h$^{-1}$ | Stable over 5 cycles | ND (SF) | 77 |
| | | | Oxidation of hydroquinones | TON = 1892; TOF = 77 h$^{-1}$ | Stable over 5 cycles | NT | 78 |
| | | | Oxidation of silanes | TON = 1880; TOF = 192 h$^{-1}$ | Stable over 5 cycles | NT | 78 |
| | | | Hydroxylamines to azoxy derivatives | TON = 1812; TOF = 33 h$^{-1}$ | Stable over 5 cycles | NT | 78 |
| | | | Oxidation of hydrazines | TON = 1812; TOF = 31 h$^{-1}$ | NT | NT | 78 |
| | | | Hydroxylamines to nitrones | TON = 293; TOF = 65 h$^{-1}$ | Significant degradation after 3 cycles | NT | 79 |
| | | | Naphthol oxidation | TON = 284; TOF = 16 h$^{-1}$ | NT | NT | 80 |
| RuRhCNT | RuRh alloyed particles of ca. 2 nm (reduction of RhCl$_3$·3H$_2$O and RuCl$_3$·6H$_2$O by heating at 160 °C in ethylene glycol/NaOH) | Electro-steric interactions | Hydrothiolation of alkenes/alkynes | TON = 14 250; TOF = 100 h$^{-1}$ | Stable over 6 cycles | ND (SF) | 81 |
| | | | Hydrophosphinylation of alkenes/alkynes | TON = 14 000; TOF = 99 h$^{-1}$ | Stable over 6 cycles | ND (SF, ICP-MS) | 82 |
| | | | Hydroboration of alkenes/alkynes | TON = 14 125; TOF = 225 h$^{-1}$ | Stable over 6 cycles | ND (SF, ICP-MS) | 83 |

3232 | *Inorg. Chem. Front.*, 2026, **13**, 3220–3236

This journal is © the Partner Organisations 2026

**Table 1** *(Contd.)*

| Hybrid | Metal species | Immobilization | Transformations | Performance metrics | Durability/stability | Leaching | Ref. |
|---|---|---|---|---|---|---|---|
| CuFe₂O₄CNTs | CuFe₂O₄ particles of *ca.* 5 nm (reduction of Cu(acac)₂ and Fe(acac)₃ by heating at 220 °C in oleylamine) | Electro-steric interactions | 1,3-Dipolar cycloaddition; Borylation of alkenes/alkynes; Selenation of quinones | TON = 880; TOF = 9 h⁻¹; TON = 8000; TOF = 80 h⁻¹; TON = 247; TOF = 14 h⁻¹ | Stable over 4 cycles; Stable over 5 cycles; NT | <2 ppm (ICP-MS); ND (ICP-MS); NT | 84; 85; 86 |
| NiCNTs | Ni(OH)₂ particles of *ca.* 2 nm ((C₂H₅)₃N·BH₃ complex-mediated reduction of Ni(acac)₂) | Electro-steric interactions | Nitroarenes to *N*-aryl hydroxylamines | TON = 571; TOF = 39 h⁻¹ | Stable over 5 cycles | ND (ICP-MS) | 87 |
| POMCNTs | Dawson-type POMs: $[P_2W_{18}O_{62}]^{6-}$ and $[P_2W_{17}Ni(OH_2)O_{61}]^{8-}$ Sandwich-type POMs: $[(P_2W_{15}O_{56})_2Ni_2(NaOH_2)_2]^{18-}$ and $[(P_2W_{15}O_{56})_2Ni_2(NiOH_2)_2]^{16-}$ | Electrostatic interactions | H₂ evolution reaction | 5.1 mA cm⁻² at −0.75 V *vs.* SCE | Stable over 9 days (LSV) | NT | 89 |
| CNT-*p*DAPy-Co | [Co(dmgH)(dmgH₂)]Cl₂] (dmgH₂ = dimethylglyoxime) | Cobalt coordination | H₂ evolution reaction | 0.4 mA cm⁻² at −0.75 V *vs.* NHE | Stable for a few h | Loss of Co | 91 |

NT: not tested; ND: not detected; SF: studied by the "stop-filtration" experiment for the removal of the solid catalyst, thus only demonstrating that the active species is attached to the CNT support; ICP-MS: studied by inductively coupled plasma mass spectrometry, thus fully demonstrating the absence of metal in solution; ORR: oxygen reduction reaction; and LSV: linear sweep voltammetry.

of the nitrogen to cobalt atomic ratio, suggesting that most pyridines were bonded to cobaloximes.

This hybrid was used as a catalyst for the hydrogen evolution reaction in fully aqueous media. The presence of surface pyridine groups on CNTs was shown to promote cobaloxime binding in the Co(III) and/or Co(II) oxidation states, thus facilitating the initiation of H₂ evolution catalysis. However, limited stability of the pyridine–cobalt bond has been observed under electro-catalytic conditions, which precludes sustained catalysis.[91]

## Conclusions and perspectives

Self-assembled polymerized lipid nanorings on CNTs emerge from this body of work as a genuinely modular and robust platform for heterogeneous catalysis, capable of immobilizing both nanoparticulate and molecular metal species while preserving the intrinsic structural and electronic properties of the carbon scaffold. Relying on a primary diacetylene-based amphiphilic layer combined, in some cases, with a secondary polycationic network, these systems enable dense, homogeneous, and firmly bound metal loading, including noble metals, base-metals, and polyoxometalates. This architecture translates into catalysts that operate under remarkably mild and sustainable conditions (room temperature, aqueous or benign solvents, and very low metal loading). Nanohybrids yet display high activity, selectivity, and recyclability in a broad array of transformations ranging from aerobic oxidations and reductive processes to C–C/C–X bond formations and electro-catalytic reactions relevant to energy conversion (see Table 1 for an overview).

Beyond demonstrating the synthetic versatility of nanoring-based lipid interfaces, the reviewed examples outline general design principles for next-generation CNT-supported catalysts: spatial confinement of reactants within lipophilic nano-reactors proximal to active sites, tunable interfacial charge and functionality to control metal anchoring and dispersion, and spatial organization compatible with flow and device integration. The successful extension to bimetallic systems, redox-active molecular oxides and cobaloximes highlights the potential of this strategy to engineer cooperative effects and to bridge the gap between molecular and materials catalysis, while microfluidic implementation illustrates a clear pathway towards continuous, scalable processes.

However, despite offering a robust anchoring for metal nanoparticles, polymerized lipidic interfaces on carbon nanotubes remain subject to some limitations that could hinder their scalability and broader use. For instance, the need for custom-made diacetylenic amphiphiles as a primer coating may prevent wider applications, as these are not yet commercially available and require a few synthetic steps. In addition, UV photopolymerization needed to reinforce the coating around CNTs introduces constraints if scale-up and industrialization are envisioned. The nanohybrid catalyst may also suffer dispersion issues in certain solvents, which limit the liquid–

This journal is © the Partner Organisations 2026

*Inorg. Chem. Front.,* 2026, **13**, 3220–3236 | **3233**

solid interfacial contact area. It may be sensitive to extreme conditions of temperature, as potential aggregation and sintering of metal nanoparticles could occur in the long-term. This would reduce the number of accessible active sites and lead to catalyst deactivation. Extreme temperatures could also induce stability issues with leaching of the metals.

Future efforts aimed at expanding the chemical diversity of amphiphilic building blocks, enhancing long-term stability under electro- and photo-catalytic regimes, and systematically correlating the nanoarchitecture with performance should consolidate polymerized lipid nanorings as a general platform for multifunctional catalytic hybrids at the interface of chemistry, energy, and materials science. Other perspectives include the development of single-atom and sub-nanometer catalysts anchored on CNTs using polymerized lipids, which could offer a promising route to maximize metal utilization and catalytic efficiency. Advances in *in situ* characterization techniques will be critical for understanding catalyst behavior, sintering mechanisms, and active sites under real reaction conditions. Additionally, integrating CNT-based catalysts into hybrid or hierarchical supports (*e.g.*, CNT–graphene or CNT–oxide composites) may improve stability and mass transport.

In addition to the heterogenization of the metal catalyst, carbon nanotube platforms offer a suitable environment for the supramolecular assembly and polymerization of other forms of catalytic species, such as organocatalyst-based amphiphiles. The latter are active in promoting organic transformations, including enantioselective ones, a direction actively pursued.[92,93]

## Author contributions

Writing – original draft: E. G.; data curation, visualization, conceptualization, funding acquisition, project administration, and writing – reviewing and editing: E. G., M. P. N., S. P., C. D., G. A. M. J., E. N. S. J., I. N. N. N. and E. D.; all authors revised and agreed with the present form of the paper.

## Conflicts of interest

There are no conflicts to declare.

## Data availability

No primary research results, software or code have been included and no new data were generated or analysed as part of this review.

## Acknowledgements

## References

1 S. Iijima, *Nature*, 1991, **354**, 56.

2 L. V. Radushkevich and V. M. Lukyanovich, *Zurn. Fisic. Chim.*, 1952, **26**, 88.

3 A. Oberlin, M. Endo and T. Koyama, *J. Cryst. Growth*, 1976, **32**, 335.

4 M. Ferrier, A. Kasumov, R. Deblock, S. Guéron and H. Bouchiat, *C. R. Phys.*, 2009, **10**, 252.

5 S. Abdelhaleem, M. Noun, N. M. Yousif and M. S. Shalaby, *Physica B: Condens. Matter*, 2025, **697**, 416704.

6 Y. Lee, H. Jung, B. Choi, J. Yoon, H. B. Yoo, H.-J. Kim, G.-H. Park, D. M. Kim, D. H. Kim, M.-H. Kang and S.-J. Choi, *RSC Adv.*, 2019, **9**, 22124.

7 J.-M. Bonard, M. Croci, C. Klinke, R. Kurt, O. Noury and N. Weiss, *Carbon*, 2002, **40**, 1715.

8 J. L. Kwo, M. Yokoyama, W. C. Wang, F. Y. Chuang and I. N. Lin, *Diamond Relat. Mater.*, 2000, **9**, 1270.

9 W. A. de Heer, A. Châtelain and D. Ugarte, *Science*, 1995, **270**, 1179.

10 M.-Y. Li and H. Peng, *ACS Biomater. Sci. Eng.*, 2025, **11**, 135.

11 E. W. Fenta and B. A. Mebratie, *Helyion*, 2024, **10**, e36490.

12 A. Allafchian and M. B. Khorzoghi, *Results Chem.*, 2025, **17**, 102538.

13 V. Schroeder, S. Savagatrup, M. He, S. Lin and T. M. Swager, *Chem. Rev.*, 2019, **119**, 599.

14 Y. Zhang, J. Guo, Z. Tang, C. Tang, Y. Li, X. Tao, B. Zhou, W. Chen, L. Guo, K. Tang and T. Liang, *Biosens. Bioelectron.:X*, 2024, **17**, 100424.

15 K. de Almeida Barcelos, J. Garg, D. C. Ferreira Soares, A. L. Branco de Barros, Y. Zhao and L. Alisaraie, *J. Drug Delivery Sci. Technol.*, 2023, **87**, 104834.

16 C. L. Brito, J. V. Silva, R. V. Gonzaga, M. A. La-Scalea, J. Giarolla and E. I. Ferreira, *ACS Omega*, 2024, **9**, 8687.

17 Y. Zhang, Y. Bai and B. Yan, *Drug Discovery Today*, 2010, **15**, 428.

18 G. M. A. Rahman, D. M. Guldi, E. Zambon, L. Pasquato, N. Tagmatarchis and M. Prato, Dispersable Carbon Nanotube/Gold Nanohybrids: Evidence for Strong Electronic Interactions, *Small*, 2005, **1**, 527.

3234 | *Inorg. Chem. Front.*, 2026, **13**, 3220–3236

This journal is © the Partner Organisations 2026

19 D. Eder, Carbon Nanotube–Inorganic Hybrids, *Chem. Rev.*, 2010, **110**, 1348.

20 B. Wu, Y. Kuang, X. Zhang and J. Chen, *Nano Today*, 2011, **6**, 75.

21 N. Karousis, N. Tagmatarchis and D. Tasis, Current Progress on the Chemical Modification of Carbon Nanotubes, *Chem. Rev.*, 2010, **110**, 5366.

22 P. Singh, S. Campidelli, S. Giordani, D. Bonifazi, A. Bianco and M. Prato, Organic functionalisation and characterisation of single-walled carbon nanotubes, *Chem. Soc. Rev.*, 2009, **38**, 2214.

23 K. Kamaras, M. E. Itkis, H. Hu, B. Zhao and R. C. Haddon, Covalent Bond Formation to a Carbon Nanotube Metal, *Science*, 2003, **301**, 1501.

24 J. L. Bahr, J. Yang, D. V. Kosynkin, M. J. Bronikowski, R. E. Smalley and J. M. Tour, Functionalization of Carbon Nanotubes by Electrochemical Reduction of Aryl Diazonium Salts: A Bucky Paper Electrode, *J. Am. Chem. Soc.*, 2001, **123**, 6536.

25 P. Luksirikul, B. Ballesteros, G. Tobias, M. G. Moloney and M. L. H. Green, Sidewall functionalisation of carbon nanotubes by addition of diarylcarbene derivatives, *J. Mater. Chem.*, 2011, **21**, 19080.

26 M. Holzinger, J. Abraham, P. Whelan, R. Graupner, L. Ley, F. Hennrich, M. Kappes and A. Hirsch, Functionalization of Single-Walled Carbon Nanotubes with (R-)Oxycarbonyl Nitrenes, *J. Am. Chem. Soc.*, 2003, **125**, 8566.

27 C. Ménard-Moyon, N. Izard, E. Doris and C. Mioskowski, Separation of semiconducting from metallic carbon nanotubes by selective functionalization with azomethine ylides, *J. Am. Chem. Soc.*, 2006, **128**, 6552.

28 V. Georgakilas, K. Kordatos, M. Prato, D. M. Guldi, M. Holzinger and A. Hirsch, Organic Functionalization of Carbon Nanotubes, *J. Am. Chem. Soc.*, 2002, **124**, 760.

29 D. Tasis, N. Tagmatarchis, A. Bianco and M. Prato, Chemistry of Carbon Nanotubes, *Chem. Rev.*, 2006, **106**, 1105.

30 R. López-Garzón, M. L. Godino-Salido, M. D. Gutiérrez-Valero, P. Arranz-Mascarós, M. Melguizo, C. García, M. Domingo-García and F. J. López-Garzón, *Inorg. Chim. Acta*, 2014, **417**, 208.

31 M. Savastano, P. Arranz-Mascarós, C. Bazzicalupi, M. Paz Clares, M. L. Godino-Salido, M. D. Gutiérrez-Valero, M. Inclán, A. Bianchi, E. García-España and R. López-Garzón, *J. Catal.*, 2017, **353**, 239.

32 A. M. Valbuena-Rus, M. Savastano, P. Arranz-Mascarós, C. Bazzicalupi, M. P. Clares, M. L. Godino-Salido, M. D. Gutiérrez-Valero, M. Inclán, A. Bianchi, E. García-España and R. López-Garzón, *Inorg. Chem.*, 2022, **61**, 12610.

33 Z. Arora, V. I. Pârvulescu, K. Philippot, J. Durand and M. Gouygou, *Catal. Sci. Technol.*, 2025, **15**, 3075.

34 H. Li, J. K. Jo, L. Zhang, C.-S. Ha, H. Suh and I. Kim, *Adv. Funct. Mater.*, 2010, **20**, 3864.

35 M. Haake, D. Aldakov, J. Pérard, G. Veronesi, A. Aguilar Tapia, B. Reuillard and V. Artero, *J. Am. Chem. Soc.*, 2024, **146**, 15345.

36 P. D. Tran, A. Le Goff, J. Heidkamp, B. Jousselme, N. Guillet, S. Palacin, H. Dau, M. Fontecave and V. Artero, *Angew. Chem., Int. Ed.*, 2011, **50**, 1371.

37 J. Schild, B. Reuillard, A. Morozan, P. Chenevier, E. Gravel, E. Doris and V. Artero, *J. Am. Chem. Soc.*, 2021, **143**, 18150.

38 S. Gentil, J. K. Molloy, M. Carrière, A. Hobballah, A. Dutta, S. Cosnier, W. J. Shaw, G. Gellon, C. Belle, V. Artero, F. Thomas and A. Le Goff, *Joule*, 2019, **3**, 2020.

39 D. Brazzolotto, Y. Nédellec, C. Philouze, M. Holzinger, F. Thomas and A. Le Goff, *Inorg. Chem.*, 2022, **61**, 14997.

40 X.-R. Li, B. Wang, J.-J. Xu and H.-Y. Chen, *Electroanalysis*, 2011, **23**, 2955.

41 L. M. Bolivar-Pineda, D. Arenas Esteban, E. V. Basiuk, S. Bals, P. Rudolf and V. A. Basiuk, *Appl. Surf. Sci.*, 2025, **709**, 163855.

42 W. Intrchom, M. Thakkar, R. F. Hamilton Jr., A. Holian and S. Mitra, *Sci. Rep.*, 2018, **8**, 153010.

43 X. Hu, T. Wang, X. Qu and S. Dong, *J. Phys. Chem. B*, 2006, **110**, 853.

44 E. Gravel, S. Foillard, H. B. Zhang, H. Y. Li and E. Doris, *Sci. China: Chem.*, 2010, **53**, 2015.

45 D. Fong, G. M. Andrews and A. Adronov, *Polym. Chem.*, 2018, **9**, 2873.

46 A. Nish, J.-Y. Hwang, J. Doig and R. J. Nicholas, *Nat. Nanotechnol.*, 2007, **2**, 640.

47 J. P. Song, S. H. Choi, D.-W. Chung and S. J. Lee, *Polymers*, 2021, **13**, 1168.

48 Y. Liu, W. Jiang, S. Li and F. Li, *Appl. Surf. Sci.*, 2009, **255**, 7999.

49 N. Mackiewicz, G. Surendran, H. Remita, B. Keita, G. Zhang, L. Nadjo, A. Hagège, E. Doris and C. Mioskowski, *J. Am. Chem. Soc.*, 2008, **130**, 8110.

50 X. Pan, R. Liu, Z. Yu, B. Haas, Z. Kochovski, S. Cao, R. M. Sarhan, G. Chen and Y. Lu, *Nanoscale*, 2023, **15**, 15749.

51 C. Richard, F. Balavoine, P. Schultz, T. W. Ebbesen and C. Mioskowski, *Science*, 2003, **300**, 775.

52 D. Astruc, F. Lu and J. Ruiz Aranzaes, *Angew. Chem., Int. Ed.*, 2005, **44**, 7852.

53 J. John, E. Gravel, A. Hagège, H. Li, T. Gacoin and E. Doris, *Angew. Chem., Int. Ed.*, 2011, **50**, 7533.

54 R. Kumar, E. Gravel, A. Hagège, H. Li, D. Verma, I. N. N. Namboothiri and E. Doris, *ChemCatChem*, 2013, **5**, 3571.

55 S. Donck, E. Gravel, N. Shah, D. V. Jawale, E. Doris and I. N. N. Namboothiri, *RSC Adv.*, 2015, **5**, 50865.

56 R. Kumar, E. Gravel, A. Hagège, H. Li, D. V. Jawale, D. Verma, I. N. N. Namboothiri and E. Doris, *Nanoscale*, 2013, **5**, 6491.

57 E. Gopi, E. Gravel and E. Doris, *Nanoscale Adv.*, 2019, **1**, 1181.

58 D. V. Jawale, E. Gravel, V. Geertsen, H. Li, N. Shah, I. N. N. Namboothiri and E. Doris, *ChemCatChem*, 2014, **6**, 719.

59 D. V. Jawale, E. Gravel, E. Villemin, N. Shah, V. Geertsen, I. N. N. Namboothiri and E. Doris, *Chem. Commun.*, 2014, **50**, 15251.

This journal is © the Partner Organisations 2026

*Inorg. Chem. Front.*, 2026, **13**, 3220–3236 | **3235**

60 D. V. Jawale, E. Gravel, V. Geersten, H. Li, N. Shah, J. John, I. N. N. Namboothiri and E. Doris, *Tetrahedron*, 2014, **70**, 6140.

61 N. Shah, E. Gravel, D. V. Jawale, E. Doris and I. N. N. Namboothiri, *ChemCatChem*, 2014, **6**, 2201.

62 N. Shah, E. Gravel, D. V. Jawale, E. Doris and I. N. N. Namboothiri, *ChemCatChem*, 2015, **7**, 57.

63 N. Shah, P. Basu, P. Prakash, S. Donck, E. Gravel, I. N. N. Namboothiri and E. Doris, *Nanomaterials*, 2016, **6**, 37.

64 P. Prakash, E. Gravel, H. Li, F. Miserque, A. Habert, M. den Hertog, W. L. Ling, I. N. N. Namboothiri and E. Doris, *Catal. Sci. Technol.*, 2016, **6**, 6476.

65 E. Gopi, V. Geertsen, E. Gravel and E. Doris, *ChemCatChem*, 2019, **11**, 5758.

66 A. Morozan, S. Donck, V. Artero, E. Gravel and E. Doris, *Nanoscale*, 2015, **7**, 17274.

67 T. N. Huan, P. Prakash, P. Simon, G. Rousse, X. Xu, V. Artero, E. Gravel, E. Doris and M. Fontecave, *ChemSusChem*, 2016, **9**, 2317.

68 J. Farah, E. Gravel, F. Malloggi and E. Doris, *J. Colloid Interface Sci.*, 2022, **613**, 359.

69 J. Farah, F. Malloggi, F. Miserque, J. Kim, E. Gravel and E. Doris, *Nanomaterials*, 2023, **13**, 1184.

70 D. V. Jawale, E. Gravel, C. Boudet, N. Shah, V. Geertsen, H. Li, I. N. N. Namboothiri and E. Doris, *Catal. Sci. Technol.*, 2015, **5**, 2388.

71 S. Donck, E. Gravel, N. Shah, D. V. Jawale, E. Doris and I. N. N. Namboothiri, *ChemCatChem*, 2015, **7**, 2318.

72 J. M. C. Tavares Junior, E. F. S. Guimarães, M. P. Nunes, R. G. Almeida, M. H. Araujo, V. F. S. Ramos, R. F. S. Menna-Barreto, J. A. Tchuiteng Kouatchou, E. Gravel, E. Doris, G. A. M. Jardim and E. N. da Silva Júnior, *ACS Omega*, 2025, **10**, 37898.

73 D. J. Jawale, V. Geertsen, F. Miserque, P. Berthault, E. Gravel and E. Doris, *Green Chem.*, 2021, **23**, 815.

74 D. V. Jawale, E. Gravel, C. Boudet, N. Shah, V. Geertsen, H. Li, I. N. N. Namboothiri and E. Doris, *Chem. Commun.*, 2015, **51**, 1739.

75 P. Basu, P. Prakash, E. Gravel, N. Shah, K. Bera, E. Doris and I. N. N. Namboothiri, *ChemCatChem*, 2016, **8**, 1298.

76 R. G. Almeida, R. L. de Carvalho, M. P. Nunes, R. S. Gomes, L. F. Pedrosa, C. A. de Simone, E. Gopi, V. Geertsen, E. Gravel, E. Doris and E. N. da Silva Júnior, *Catal. Sci. Technol.*, 2019, **9**, 2742.

77 D. V. Jawale, E. Gravel, N. Shah, V. Dauvois, H. Li, I. N. N. Namboothiri and E. Doris, *Chem. – Eur. J.*, 2015, **21**, 7039.

78 S. Donck, E. Gravel, A. Li, P. Prakash, N. Shah, J. Leroy, H. Li, I. N. N. Namboothiri and E. Doris, *Catal. Sci. Technol.*, 2015, **5**, 4542.

79 P. Prakash, E. Gravel, D.-V. Nguyen, I. N. N. Namboothiri and E. Doris, *ChemCatChem*, 2017, **9**, 2091.

80 R. L. de Carvalho, G. A. M. Jardim, A. Santos, M. H. Araujo, W. X. C. Oliveira, A. C. Bombaça, R. F. S. Menna-Barreto, E. Gopi, E. Gravel, E. Doris and E. N. da Silva Júnior, *Chem. – Eur. J.*, 2018, **24**, 15227.

81 D. V. Jawale, J.-A. Tchuiteng-Kouatchou, F. Fossard, F. Miserque, V. Geertsen, E. Gravel and E. Doris, *Green Chem.*, 2022, **24**, 1231.

82 D. V. Jawale, F. Fossard, F. Miserque, V. Geertsen, E. Doris and E. Gravel, *Catal. Sci. Technol.*, 2022, **12**, 4983.

83 M. P. Nunes, D. V. Jawale, F. G. Delolo, M. H. Araujo, E. Gravel, E. Doris and E. N. da Silva Júnior, *Chem. Commun.*, 2023, **59**, 2763.

84 P. Prakash, R. A. Kumar, F. Miserque, V. Geertsen, E. Gravel and E. Doris, *Chem. Commun.*, 2018, **54**, 3644.

85 M. P. Nunes, L. A. Machado, H. D. R. Calado, G. A. M. Jardim, J. A. Tchuiteng Kouatchou, V. Geertsen, Y. Yuan, E. Doris, E. N. da Silva Júnior and E. Gravel, A swift and efficient approach to boron-functionalized scaffolds: borylation of alkenes and alkynes using a carbon nanotube–copper ferrite catalyst, *Catal. Sci. Technol.*, 2025, **15**, 3445.

86 G. A. M. Jardim, Í.AO. Bozzi, W. X. C. Oliveira, C. Mesquita-Rodrigues, R. F. S. Menna-Barreto, R. A. Kumar, E. Gravel, E. Doris, A. L. Braga and E. N. da Silva Júnior, *New J. Chem.*, 2019, **43**, 13751.

87 P. Prakash, D. De Masi, V. Geertsen, F. Miserque, H. Li, I. N. N. Namboothiri, E. Gravel and E. Doris, *ChemistrySelect*, 2017, **2**, 5891.

88 H. N. Miras, J. Yan, D.-L. Longa and L. Cronin, *Chem. Soc. Rev.*, 2012, **41**, 7403.

89 D. V. Jawale, F. Fossard, F. Miserque, V. Geertsen, A.-L. Teillout, P. de Oliveira, I. M. Mbomekallé, E. Gravel and E. Doris, *Carbon*, 2022, **188**, 523.

90 G. Smolentsev, B. Cecconi, A. Guda, M. Chavarot-Kerlidou, J. A. van Bokhoven, M. Nachtegaal and V. Artero, *Chem. – Eur. J.*, 2015, **43**, 15158.

91 S. Donck, J. Fize, E. Gravel, E. Doris and V. Artero, *Chem. Commun.*, 2016, **52**, 11783.

92 M.-D. Hoang, R. A. Kumar, D. A. Buisson, W. L. Ling, E. Gravel and E. Doris, Self-assembled Polydiacetylene Nanoribbons for Semi-heterogeneous and Enantioselective Organocatalysis of Aldol Reactions in Water, *ChemCatChem*, 2020, **12**, 1156.

93 C. Demeese, C. Lods, D.-A. Buisson, E. Gravel, I. N. N. Namboothiri and E. Doris, Supramolecular assembly of proline amphiphiles on carbon nanotubes as heterogenized catalyst for enantioselective aldol reactions in water, *Chem. Eng. J.*, 2023, **476**, 146702.

3236 | *Inorg. Chem. Front.*, 2026, **13**, 3220–3236

This journal is © the Partner Organisations 2026